COMPUTATIONAL MODELING OF THE RAT HIPPOCAMPUS

FOR IMPROVING NEURAL STIMULATION

by

Andrew Gilbert

A Senior Honors Thesis Submitted to the Faculty of
The University of Utah
In Partial Fulfillment of the Requirements for the

Honors Degree in Bachelor of Science

In

Electrical Engineering

Approved:

Gianluca Lazzi, PhD Thesis Faculty Supervisor	Gianluca Lazzi, PhD Chair, Department of Electrical and Computer Engineering
Neil Cotter, PhD Honors Faculty Advisor	Sylvia D. Torti, PhD Dean, Honors College

April 2016

ABSTRACT

Neural prostheses are used to restore some level of function to tissue damaged by disease. It is important to model and correctly identify the relationship between electrical stimulation and neural response to provide a framework for prosthetic stimulation. This work will show a structure for conducting that analysis with several models and experimental setups presented. Specifically, a multi-scale modeling approach is employed where the admittance method is used to simulate the voltage distribution through the tissue and Neuron software is used to simulate the resulting cell response. Results will include an analysis of the effects of capacitance, heterogeneous resistivity, electrode depth, ephaptic coupling, and a presentation of a bi-directional communication simulation strategy between the admittance method and Neuron.

CONTENTS

LIST OF FIGURES

LIST OF TABLES

CHAPTER 1

INTRODUCTION

An action potential describes a spike in the membrane potential of a neuron which is transmitted rapidly along the length of an axon. The mechanism of this transmission is the intake and release of charged potassium and sodium ions through gates and pumps in the neuron membrane. When an action potential occurs, that neuron is said to have ”fired” and it is the spatial-temporal patterns of these firings in a network of neurons which compose the brains thoughts, emotions, and memories.

Specifically, the hippocampus is the segment of the brain associated with consolidating short-term memory into long-term memory. Damage to the hippocampus can cause detrimental memory-loss and decreased cognitive function [1]. This is particularly relevant for those suffering from Alzheimer's disease, dementia, cerebrovascular disease, or traumatic brain injury. While there exists a wide range in the severity of these diseases, they often result in long-term physical, emotional, and behavioral effects, with an accompanying decrease in quality of life.

Memories are encoded in spatial-temporal patterns through the hippocampus, progressing from the Dentate Gyrus (DG) through the CA3 to the CA1 [2]. A disconnect between the CA3 and CA1 results in severe memory loss and long-term disruption of memory formation [3]. For example, when rodent hippocampi are impaired, rodents show a lack of spatial learning and recall[4]. One potential solution to this problem is a neural prosthetic to enhance and restore memory. This prosthetic was developed and tested in an experimental study [3]. The prosthesic was built by creating a multi-input multi-output model to extract and estimate the firing pattern transformations between the CA1 and CA3. With a supplied input from CA3 recording electrodes and a known transformation for creating associated output firing in the CA1, the CA1 can be electrically stimulated appropriately. This model

is instantiated using software or custom VLSI hardware that is attached to upstream recording electrodes and downstream stimulating electrodes. In this configuration, the prosthesis can substitute for biological communication [3].

While the prosthesic has shown success in restoring memory, [5] there are still factors that need to be resolved. One aspect that is not well understood is the optimal stimulation magnitudes, and resulting firing patterns, required to effectively replicate memory function and specific memory codes. Before prostheses can transition in a widespread manner to humans, it is crucial to understand the threshold for electrical current levels. With this understanding, the minimum current necessary to cause a neural activation can be accurately predicted, and damage to surrounding neural tissue can be understood and minimized.

In this work, I propose a series of complex computational models to study stimulation parameters. This includes a model of an in-vitro slice of the hippocampus (slice model) and a model of a full rat hippocampus incorporating a prosthesic implanted in a hippocampus (3D model). Both models were heterogeneous and segmented such that the more resistive cell bodies were modeled appropriately in comparison with the rest of the morphology. This series of models were used to simulate the propagation of current through the tissue using a multi-resolution admittance method to convert the discretized model to a circuital network and solve for the fields and potentials from current stimulation at each of the electrodes.

Several methods were used to simulate neural activity due to this applied stimulation. First, the activating function was applied to the resulting potentials to determine the activation patterns parallel to the rostrocaudal plane. Second, a realistic CA1 pyramidal cell model was taken from a previously published study [6], and used to simulate specific neural response and firing thresholds of a neuron using Neuron software [7].

Using these strategies, I first show how this framework can be used to investigate the importance of model capacitance and the effects of resistivity variations within the models. Next, I present an evaluation of the effects of depth of electrode placement. Subsequently, I introduce an analysis of how the effects of ephaptic coupling would change the thresholds of neural stimulation. Finally, I demonstrate a framework for a bi-directional communication system between admittance method simulations of current propagation and Neuron simulations of neural response.

The significance of the set of models and frameworks presented here is the introduction of a toolset for the design of power efficient and low dimension neural prostheses.

CHAPTER 2

MODELING

This section describes the creation and specifics of models used throughout this work. First, the development of tissue models used to simulate the spread of current through tissue is discussed. Second, models of neural activation are covered.

2.1 Tissue Models

Two tissue models in particular were used during this study. First a "slice model" was developed where the model represented a 400 μm thick slice taken through the coronal (z) axis of the rat hippocampus. This is shown in Fig. 2.1 and described in Section 2.1.1.

A second model was later developed which contained additional information in the coronal plane, representing the entire rat hippocampus rather than just a portion of it. This is the "3D model" and is shown in Fig. 2.2 and described in Section 2.1.2.

There were several steps required to develop computational models. In this case those models were developed to fit the the customized simulation framework described subsequently. The input to this framework was a series of voxels where each voxel describes a region of tissue and the electrical properties associated with that region. Therefore, the first step in the creation of the models was the construction of the shape and layout of the tissue using sets of experimental data. The data contained information on the positioning of the subsections and layers of the hippocampus which then was linked to resistivity and capacitance data from separate studies. While the data was taken from one animal and can vary across a species it gave a good overview of relative structure and positioning. This experimental data was extracted, each voxel was assigned an index, and each index was associated with a tissue type and specific electrical properties. A significant body of work was devoted toward processes to create, shift, rotate, merge, and otherwise manipulate these models.

2.1.1 Slice Model - Physical Layout

The slice model was built from the segmented digital atlas published by Kjonigsen et al. [9]. Their atlas contained high resolution images (1.4 pixels/μm) of slices through the coronal (z) plane of the rat brain. The slices were stained for increased visibility and then digitally annotated to show the separate subdivisions of the hippocampus. A custom Matlab function was written to threshold each image, extracting the segmentation and converting it to the voxelized format described above. Each slice was checked for accuracy and manually adjusted using Adobe Photoshop. The data used for this model was 12 μm in all dimensions but only contained variation in tissue type in the the sagittal and transverse (x and y respectively) axes. A pair of stimulating electrodes were placed in the crest of the Dentate Gyrus (DG) to match experimental studies (as shown in Fig. 2.1). The final model size was $365 \times 175 \times 55$ voxels.

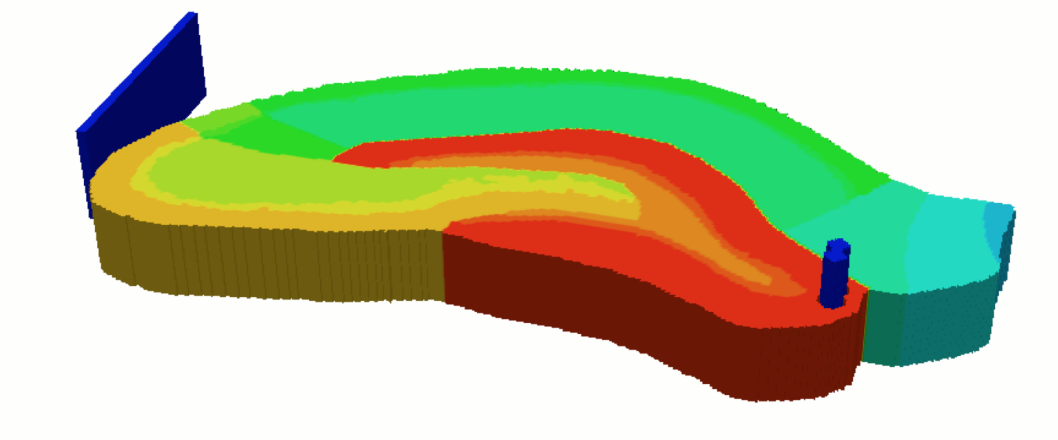

Figure 2.1: Image of the slice model where the variation in colors describes the differences in tissue type. The dark blue represents the implanted stimulating electrodes and ground plate.

2.1.2 3D Model - Physical Layout

The 3D model was created from a dataset based on a combination of MRI, immunomarker, and histochemical data from a study of a rat hippocampus, classifying 10×10^6 different points according to their position, section of hippocampus, and layer [10]. Software was written to convert the data into a 16 μm resolution 3D matrix of cubic voxels. Voxels that were undefined in the original dataset were interpolated and assigned a tissue type

based on the surrounding material. However, this method did not eliminate larger natural spaces that occur in the hippocampus due to irregularities or connections to surrounding tissue. The initial dataset also contained voxels that were separated by as little as 4 μm in the x and y dimensions and 16 μm in the z dimension. To increase computational speed and maintain uniform dimensions, the resolution was set to 16 μm in all dimensions. A 2×8 electrode array, mimicking the prosthetic, was inserted into the model with one row of electrodes in the CA1 and another in the CA3. Each electrode was 48 μm in diameter with a 32 μm layer of insulation. The prosthetic model was implanted near the septal pole with each row was parallel to the mediolateral plane. The final model size was $475 \times 500 \times 288$ voxels.

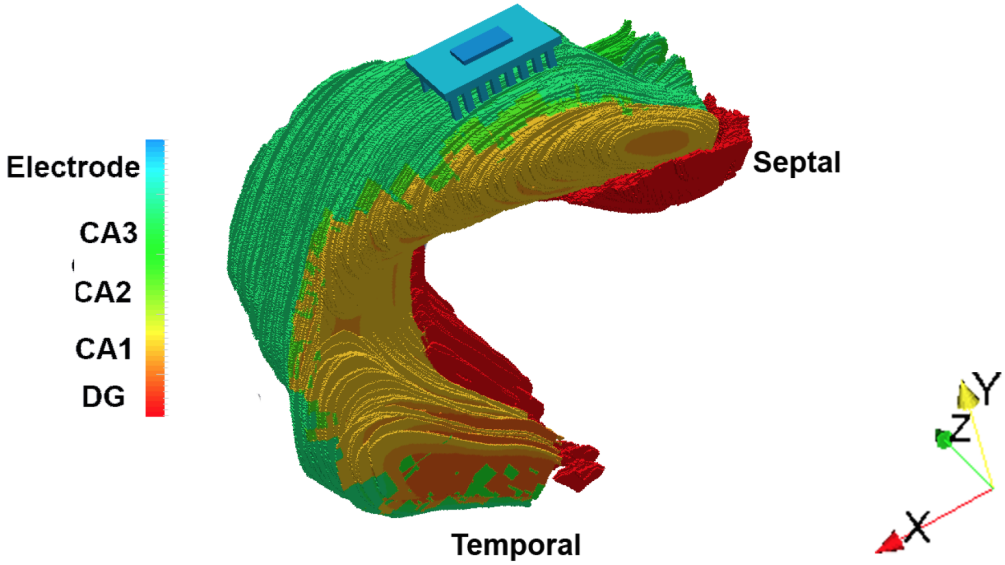

Figure 2.2: Image of the 3D model where the variation in colors describes the differences in tissue type. The blue represents the implanted model of the prosthetic.

2.1.3 Electrical Properties

For both models, the material index assigned to each voxel corresponded to its section and layer, where the section refers to CA1, CA2, CA3, or DG, and the layer refers to either the the Lacunosum-Moleculare (LM), Radiatum (RAD), Pyramidal Cell (PC), or Oriens (OR). These subsections and layers are delineated in Fig. 2.3. The different layers represent regions containing separate sections of the neurons in the hippocampus. In other words,

the neurons within the hippocampus are generally parallel to each other, arranged radially following the shape of the CA and DG with the cell bodies (PC layer) at the same depth (or layer). As the cell bodies are comparatively large this layer is more densely packed and thus the resistivity is much higher than the surrounding layers composed of dendrites. In these models that segmentation is important because the varying resistivity will affect the spread of current through the tissue.

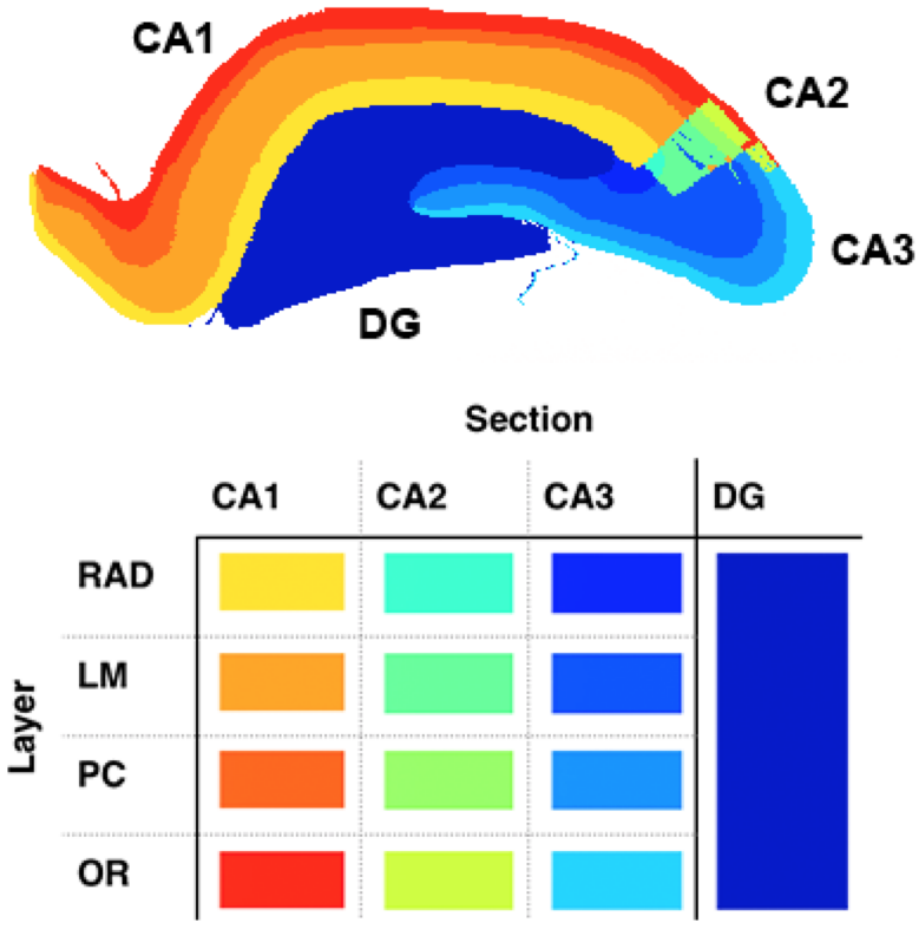

Figure 2.3: The sections and layers of the hippocampus are delineated to show how the models were segmented.

Each index was assigned an impedance (composed of resistivity and capacitance) which is the measure of how difficult it is for current to flow through that voxel. The impedance

can vary in the x, y, and z direction to allow for tissue anisotropy although in this case none was introduced. In this case the tissue was modeled as purely resistive because the dominant frequency of the stimulation pulse lies in the low frequency range, although this hypothesis was validated through experimentation which is described in more detail later. For the models described in this work, tissue properties of the hippocampus were taken from Lopez-Aguado's in-vitro study of the CA1 [11] and those resistivity values are shown in Table 2.1.

Section	**Resistivity (Ω-m)**
OR	3.215
PC	6.4291
LM	2.6045
RAD	2.8792
Surrounding Tissue	3.215

Table 2.1: Material resistivity values [11]

2.2 Simulation

This section describes the simulation methods used to solve the models described above.

2.2.1 Meshing and Netlist Creation

The model was then meshed and converted to a circuital network. The meshing process was used to increase computational speed by combining large sections of tissue that are composed of the same material into larger voxels and adjusting the corresponding resistivity and capacitance of the new voxel. This leads to a smaller set of components which decreases the required processing time to solve the model. However, the meshing algorithm leaves a high resolution near material boundaries, preserving the accuracy of the model. The meshed model is then used to generate a circuit of resistors and capacitors connecting every remaining node. The value of these components was set to represent the impedance between each pair of nodes and was determined from the positional relationship of the nodes, the average conductivities of the materials in neighboring voxels, and the distance between them. For example, the admittance (the inverse of impedance) for a node at *i, j,*

k in the x direction is shown in Equation 2.1 where σ refers to the calculated conductivity from Table 2.1 [14] [8].

$$g_x^{i,j,k} = \sigma_x^{i,j,k} * \frac{\Delta x}{\Delta y \Delta z} \tag{2.1}$$

This circuit was the input to the admittance method. Current sources were input at the location of each electrode to serve as the stimulus for the model. This meshing and network generation process is shown in Fig. 2.4. The programs to perform this as well as the admittance method described in the subsequent section were developed my Carlos Cela during his doctoral work [8], but are presented here for background.

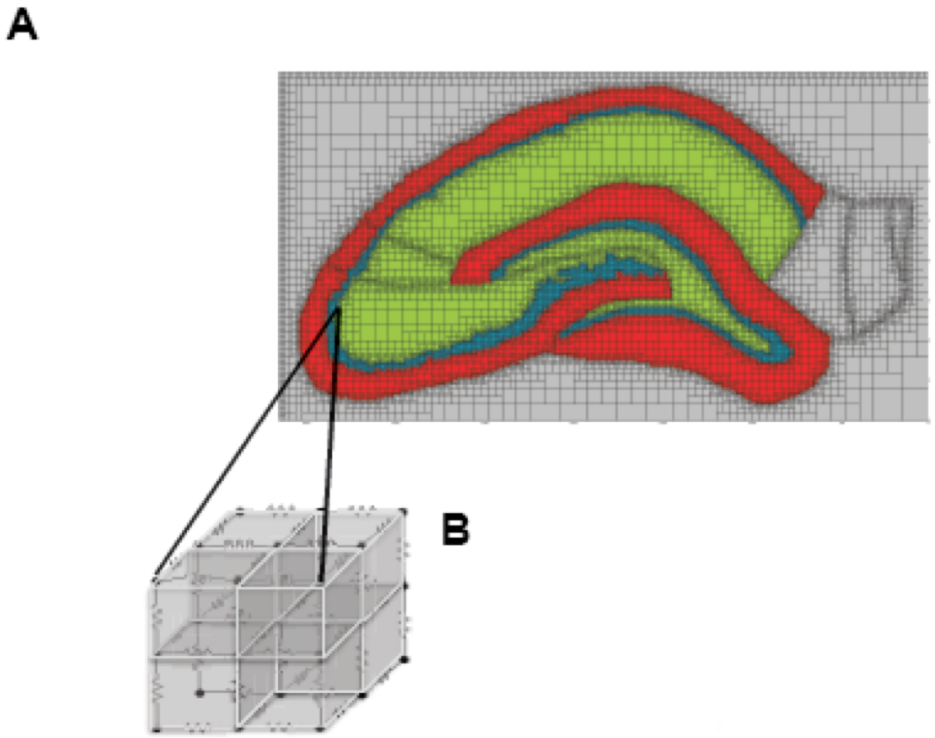

Figure 2.4: The pre-processing steps of the admittance method: A) meshing where large areas of homogeneous tissue are combined into larger voxels and B) network generation where each voxel is transformed into a resistor cube with resistances determied by the conductive properties of the adjacent tissue. Images modified from [12]

2.2.2 Admittance Method

The admittance method was originally proposed by Armitage in 1983 [13] and was implemented in the Lazzi lab by Cela in 2011 [14]. An admittance (inverse of impedance) matrix G was formed from the netlist of the above circuit to describe the admittance between every node in the circuit. This matrix will be sparse as only specific connections were described in the netlist. Current sources were contained in a vector I and together G and I define the relationship between all nodes in the network. The voltages (V) at each node in the circuit were then solved using G, I, Equation 2.2, and the biconjugate gradient method [14] [8].

$$G * V = I \tag{2.2}$$

After the simulation, the voltages at each node were obtained. These results were then run through an interpolation routine to find the voltages in the center of each voxel based on the surrounding nodes. The electric field throughout the model was then determined from the first spacial derivative of the voltage. This field was used to solve for current density through the model using Equation 2.3 [14] [8].

$$J = \sigma * E \tag{2.3}$$

2.2.3 Activating Function

The activating function was originally proposed by Rattay in 1986 [15]. The activating function characterizes the response of an axon due to electrical stimulation to predict neural stimulation. It is calculated as shown in Equation 2.4 where V_e defines the voltage along the axon and f is the resulting activating function [15].

$$f = \frac{\partial^2 V_e}{\partial x^2} \tag{2.4}$$

Positive values of Equation 2.4 correlate to axonal activation. The activating function is often used to give an initial estimation for axonal activation due to external stimulation. Of course, since the electric field is linearly proportional to the current density as shown in Eq. 2.3 and the electric field is equal to the first spatial derivative of the voltage this means that neural activation is also proportional to the first spatial derivative of the current density.

2.3 Neuron Modeling

Neuron behavior is complicated, but neurons can also be modeled as an electrical system. Models of this type were first created by Hodgkin and Huxley [16]. Hodgkin and Huxley's method represented a neuron as similar to a transmission line, or as a series of compartments where each compartment is composed of two rails (an intracellular and extracellular rail) and several conductances and voltage sources in parallel with a capacitor between the rails to describe the cell membrane. Each conductance and voltage source represent an ionic mechanism which controls the flow of specific ions through the cell membrane. By including a conductance for each ionic mechanism in a cell, a modeler can create an extremely accurate representation of a cell. The compartments are connected with series resistances as shown in Fig. 2.5. The inside rail represents the voltage inside the cell while the outside rail represents the membrane voltage. If an external stimulus of large enough magnitude is applied to the outside of the cell, then the cross-membrane voltage will propagate along the axon in both directions, modeling an action potential. These models can also be connected with complex models of the propagation of neurotransmitters between cells, or synapses.

However, several other models do exist. For example neuron behavior can be described by a simple leaky integrate and fire (LIF) model where the neuron is represented by a single membrane potential. If this membrane potential grows greater than a certain threshold the neuron will "fire" and release a spike to all connected neurons (post-synaptic connections). Any neuron's potential can be increased or decreased by the firing of those neurons connected to it (pre-synaptic connections). The advantage of this model is that it is computationally efficient. Whereas the Hodkin-Huxley (HH) model requires the solution of numerous Ordinary Differential Equations (ODEs) at every time step, the LIF requires only a series of sums. This allows complex networks of neurons to be simulated and overall network behavior to be evaluated. Additionally, there are various other models which grow in complexity and accuracy from the LIF to HH. While the evaluation of network behavior would be advantageous, the crucial drawback of the LIF and other models is that while parameters may be adjusted to ensure accurate network behavior, individual behavior is inaccurate. Additionally, the LIF lacks a spatial dimension. In the HH model each compartment can be linked to a specific location in space and the local field effects

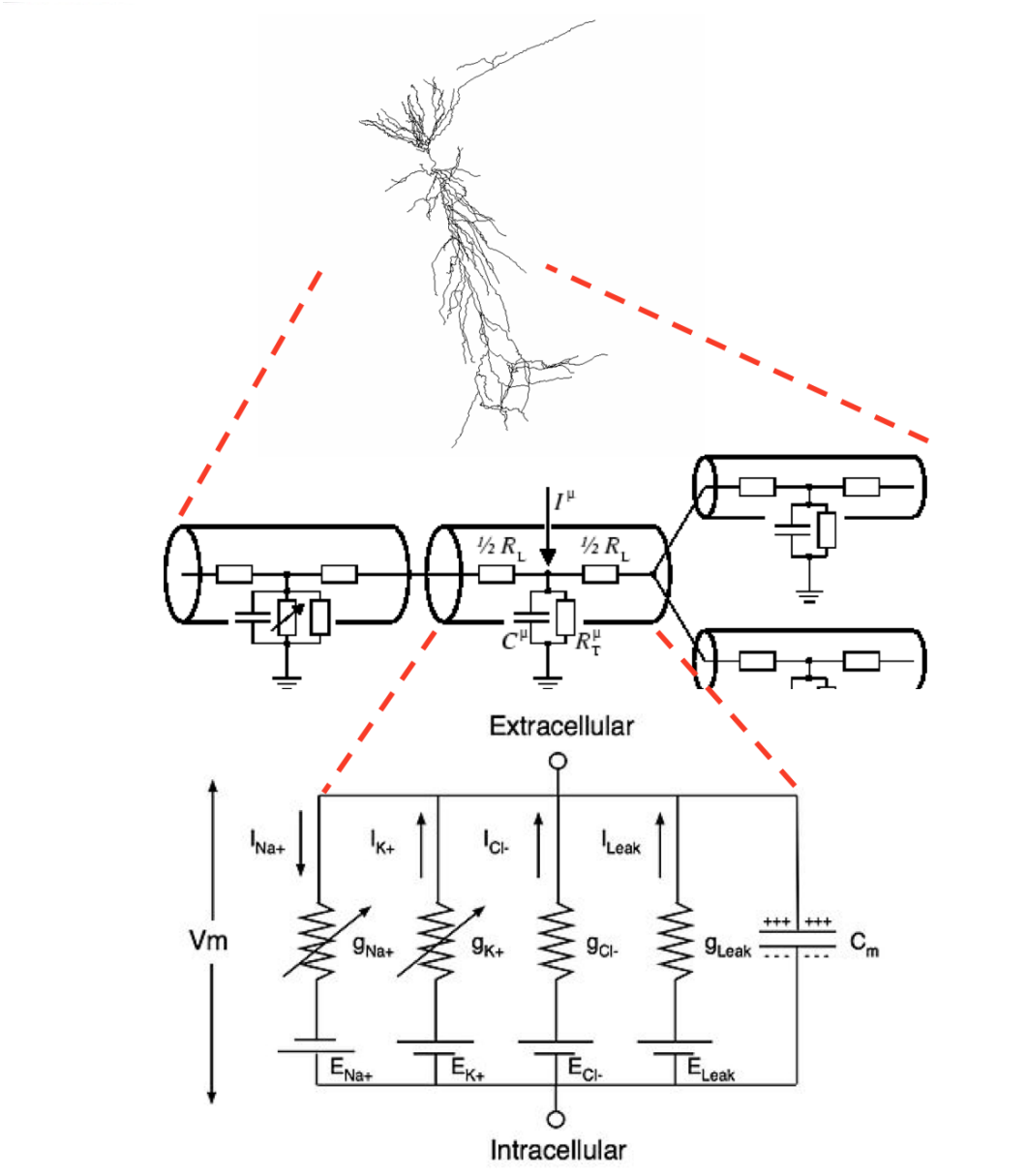

Figure 2.5: Electrical model of neuron simulation. The model is composed of a series of compartments with each compartment composed of a a capacitor in parallel with series conductances and voltage sources to represent the voltage across the membrane. Each of the compartments are connected by series resistances. Images modified from [6], `http://icwww.epfl.ch/`, and `http://wikipedia.org/`

around that compartment can be applied. Moreover a network of HH neurons can be developed, it just requires a high degree of computational power to simulate. Because computational speed was not an issue while accuracy was a high priority, HH models will be used exclusively in this work.

2.3.1 Single Cell Model

The cell used primarily in this work was an HH model of a CA1 pyramidal cell [6]. This model was chosen because of its realistic attributes and calibration. First, the morphology was taken from several in-vitro studies making it a good choice when studying the effects of spatial potential fields. Second, it includes a series of voltage dependent ionic channels to accurately describe membrane response. Third, the model parameters were set by comparing to experimental data from both a 50 Hz spike train input and a single discrete impulse. Although the methodology presented here uses a biphasic current pulse, the response should be similar to that of a discrete impulse indicating that the parameters should be already set for these experiments.

2.3.2 Cell Network Model

The tissue models also have the capability to be integrated with large-scale network models [2] as shown here [12]. The large scale model was not used in results presented here due to the ongoing nature of that work, the focus of that model on the DG while the CA1 is emphasized here, and the greater ease of interpreting results with only a single cell, but the capability to integrate with a network model is present and has been implemented.

2.4 Multi-scale modeling

There is a direct relationship between the level of detail within a simulation and the amount of time that the simulation will take to run. While super-computers and the parallelization of code can help to alleviate this problem, large scale simulations of highly detailed models are a difficult task. Moreover, different models can be developed for analyzing different aspects of tissue response. For example, while HH models or the activating function can be used to evaluate neural response to external simulation, they are unable to show how current spreads through the tissue. Meanwhile, admittance models can show how current spreads, but give no insight into neural response. Therefore, throughout this work a multiscale approach was used to obtain an impression of the response of cells in a specific location within the hippocampus.

In this approach the admittance method was used to simulate the spread of current and the resulting voltage at each point in the tissue. Those voltages were then interpolated at the locations of the center of each neuron compartment in an HH model. The response

of the neuron model was observed by applying those voltages as extracellular voltages within Neuron. The neuron model was shifted throughout the tissue model to observe how spatial variation might effect response or the amplitude of the stimulation can be varied to determine the threshold level of response for the neuron.

The multi-scale methodology used in this work is shown in Fig. 2.6.

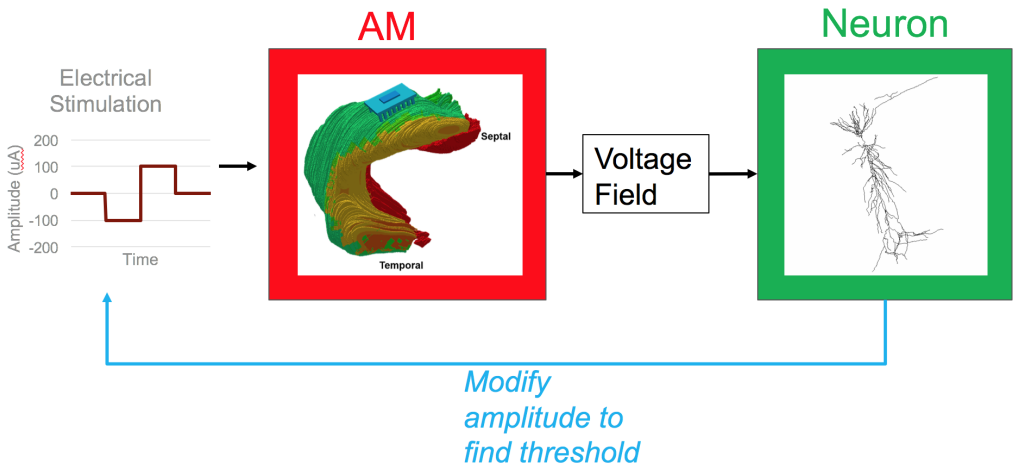

Figure 2.6: In a multi-scale simulation the admittance method is first used to simulate the potential field through a region of tissue. Afterwards the voltage is interpolated at the center of each neuron compartment and applied as an extracellular voltage. The input current to the admittance method can be varied to test for neural response thresholds

CHAPTER 3

EXPERIMENTS

This chapter will evaluate various assumptions that served as a baseline for this work as well as the effects of varying model parameters.

3.1 Effects of Model Capacitance

Throughout the experiments described in this work the quasi-static approximation was used. This approximation assumes that capacitive, inductive, and wave propagation effects within neural tissue are negligible. Plonsey and Heppner [17] provided the original analysis of why this assumption should hold valid for the lower frequencies (1-10kHz) used in neural stimulation. The approximation greatly simplifies the necessary calculations to determine the field distribution through tissue and thus it has been used extensively by the neural modeling community. A theoretical analysis of the effect of tissue capacitance, showing why it is negligible in low-frequency neural simulations is presented in Appendix A.

However, some recent studies have indicated that for some experimental parameters, the effect of added tissue capacitance may not be negligible. For example, several studies showed that added capacitance to the tissue may have a filtering effect on the neural signals [18] [19]. Butson *et al* [20] showed that in simulations of deep brain stimulation, added tissue capacitance could lead to a 20% decrease in the volume of tissue activated. Finally, Bossetti *et al* [21] were able to show that an error of 5-13% between solutions to models using the quasi-static approximation and those without it. The magnitude of the error depended on pulse length and pulse amplitude with shorter lengths and larger amplitudes increasing error. When applied to neural activation, errors of 0-9% were shown in the threshold distance curves. The error was due to differences in the phase of the impedance as the magnitude of the impedance did not change with added capacitance.

These studies showed that the magnitude of the error between simulations using capacitive properties and those that do not has been shown to have a positive correlation with stimulation amplitude and dielectric constant value. With the stimulation parameters used in the following studies (amp $\approx$ 100 μA, width = 1 ms, $\epsilon_r \approx 1.5 \times 10^5$) capacitance is unlikely to play a significant role because the parameters are smaller than those presented in the above studies. However, this assumption was first validated with several experiments that introduced capacitance into the model and compared results to control studies without capacitance.

3.1.1 Methods

Experiments testing the effects of added capacitance were performed on both the 3D model and the slice model for validation, although only the slice model experiments will be described here. Results were similar across the models.Table 3.1 shows the parameters of each of the experiments performed. The electrode capacitance describes the capacitance of the interface between the electrode and tissue. The values chosen were based on those experimented with in [20] which were judged to be typical for neural stimulation. The values for the dielectric constant were taken from [22]. Each of the experiments had a pulse amplitude of 100 μA. Variations in the capacitance were introduced to evaluate the applicability of results to new stimulation cases as well as account for natural variations in real parameter values.

Experiment	**Tissue Capacitive Properties**	**Total Electrode Capacitance**	**Pulse Duration**
Control	None	None	1 ms
A	None	1uF	1 ms
B	None	3.3uF	1 ms
C	Grey Matter at 1kHz	1uF	1 ms
D	Grey Matter at 10kHz	1uF	100 us

Table 3.1: Experimental parameters of the various capacitance experiments performed

3.1.2 Results

All of the experiments showed very little difference with the control setup. The Pearson product-moment correlation coefficients between the datasets was 99% while the normalized root mean squared error (normalized based on the range of data recorded) was less then 100 μv for all cases. These results indicate that for the stimulation parameters used in this work capacitance can safely be ignored. This is advantageous because it increases computational speed and it means that results will scale linearly with input current, which is useful for determining thresholds of neural activation.

3.2 Resistivity Variation

While Bossetti *et al* showed capacitive properties had relatively no effect on the magnitude of the impedance, conductivity had a linear effect on the magnitude in their results (see Appendix A for a further analysis on this point) [21]. Therefore, the conductivity should have a linear effect on the voltage field and the current density. The relative effect of heterogeneous tissue should therefore depend on the level of variation in resitivity across the tissue. Current will be pushed away from areas of high resistivity, while it should spread evenly in areas of homogeneity. One of the benefits of using the admittance method for simulation is the feasibility of creating a complex heterogeneous model and varying the parameters. To test the relative importance of heterogeneity, a sensitivity analysis was performed to analyze varying resistivity distributions within the hippocampus.

3.2.1 Methods

The resistivity values used throughout this work were taken from the study published by Lopez-Aguado *et al* [11] shown in Table 2.1. These values were recorded from the CA1, but due to the lack of resistivity data for the rest of the hippocampus the values were applied to the other hippocampus sub-sections as well. Within the hippocampus, most layers are near homogeneous, with the exception of the cell body (PC) which is more than double the other layers. This is because the PC region is much more densely packed due to the size of the cell bodies compared to the dendrites. The PC layer is highlighted in the Fig. 3.1.

In a set of seven studies, the PC resistivity was varied so that the ratio between PC resistivity to LM resistivity was $\times 1$ (homogeneous), $\times 2$, $\times 2.23$ (original ratio, control test), $\times 3$, $\times 4$, $\times 5$, and $\times 10$. Each study was analyzed to view how it compared to the

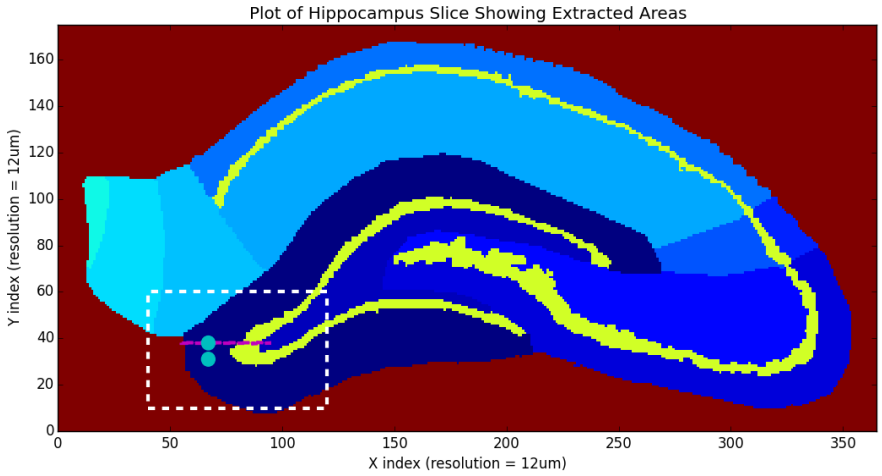

Figure 3.1: Location of the Pyramidal Cell (PC) layer within a slice of the rat hippocampus. The PC layer is highlighted in light green. The white dotted box shows the location of the boundaries of Fig. 3.2a and Fig. 3.2b while the magenta line represents the axis of the plot in Fig. 3.3a. The two teal circles inside the white dotted box represent the locations of the two stimulating electrodes

control test. A biphasic current pulse with a duration of 1 ms and an amplitude of 100 μA was used for stimulation.

3.2.2 Results

Results showed that changing the PC resistivity did have an effect on the flow of current through tissue. Figs. 3.2 and 3.3 show the relative effect on current density for each experiment. Specifically, Fig. 3.2a shows the spread of current density in each experiment. Of course the majority of the current is clustered directly beneath the stimulating electrodes (for reference the location of the electrodes with respect to the boundaries of the plots in Fig. 3.2 is shown in Fig. 3.1). However, it is evident that the experiments with a larger heterogeneity block current from entering the PC layer and thus passing through the layer into the hilus region (the region inside the PC layer) while the homogeneous ($\times 1$) experiment allows the current to spread evenly through the PC and hilus. Fig. 3.2b shows the difference in current density magnitude between each experiment and the control study. While there is an increasing magnitude of difference within the PC layer as the heterogeneity increases, there is also an increase outside of the PC layer in the area beneath the electrode, showing that changing heterogeneity would have effects on current flow

throughout the hippocampus and not just within the PC layer.

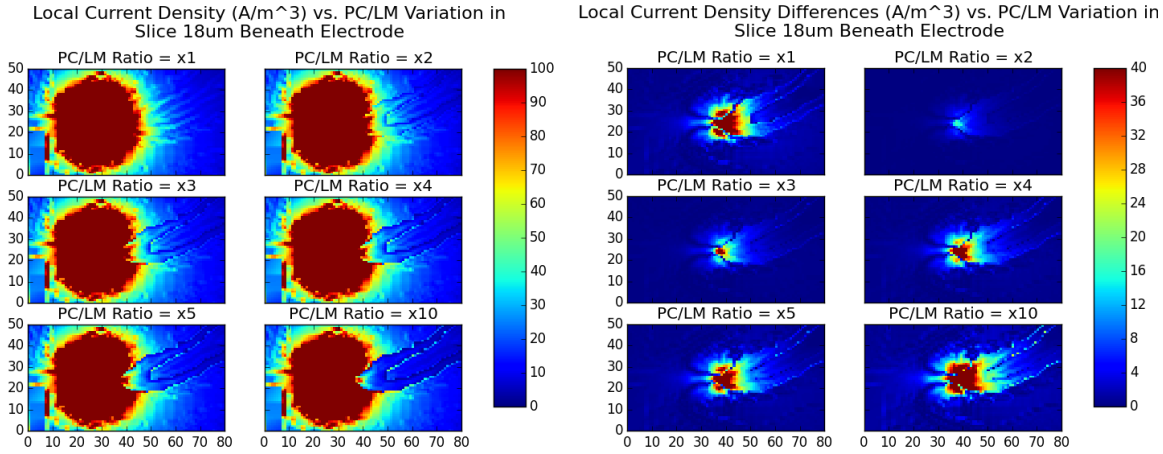

(a) Current density through each of the experimental studies

(b) Difference in current density in each experimental study and the current density through the control

Figure 3.2: Current density results from each experiment (borders of the plots are shown by the white dotted line in Fig. 3.1)

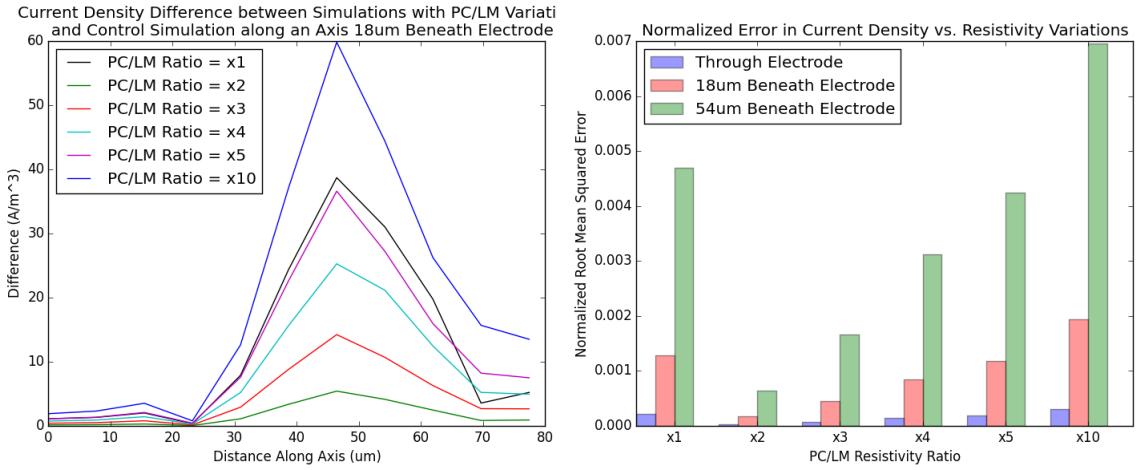

(a) Difference in current density for each experimental study and the current density through the control. The axis of this plot is shown in Fig. 3.1

(b) The magnitude of the normalized Root Mean Squared Error (RMSE) between the current density in each experiment and the control simulation at a depth taken through the electrode, 18μm beneath the electrode, and 54 μm beneath the electrode.

Figure 3.3: Current density variations for each experiment

Fig. 3.3a shows the relative magnitude of the difference in current density between each experiment and the control along the axis shown in magenta in Fig. 3.1. The difference is minimal at the electrode location ($\approx$ 20 μm along the axis) and reaches a peak inside the PC layer as expected. The homogeneous solution has a slightly higher magnitude of error through most of the tissue than the PC/LM ratio = $\times$ 5 experiment. However, as the axis moves into the hilus region (greater than $\approx$ 70 μm) the error is smaller. Figs. 3.2 and 3.3a were both taken at a depth of 18μm beneath the electrode. Finally, Fig. 3.3b shows how these results would change with increasing or decreasing depth The normalized Root Mean Squared Error (RMSE) between the current density for each experiment in the area shown in Fig. 3.1 and the current density between the control in that same area is shown at three different depths. The RMSE was normalized with respect to the range of the data for Fig. 3.3b shows that the error would grow with increasing depth beneath the electrode. However, the magnitude of the current density would also shrink in this region, indicating that the error is less significant.

For reference, a difference of 60 A/m^3 corresponded to an approximate difference of 14 mv within the PC region while 40 A/m^3 corresponded to a difference of 10 mv. While the magnitude of the voltage field is not an accurate measure of neural activation, studies have shown that a depolarization of $\approx$15mv can cause a response in a hippocampal pyramidal cell [23]. This indicates that large variations in resistivity could cause differences in neural activation thresholds. However, the effect is small enough that some small error in the measurements used would not have a large effect on the results shown here, indicating that these studies should be still be applicable for varying experimental data. This study indicates that heterogeneous resistivity would have an estimated effect on neural activation and current flow in certain cases but not others.

3.3 Depth of Electrode placement

One of the factors that effects neural response is the location of electrode placement. Because the shape and formation of the hippocampus, as well as the nature of memory loss, will be different for every animal, it is impossible to exactly determine an optimal location for the stimulating electrode. However, due to the heterogeneous nature of the hippocampus tissue, the depth of electrode placement may play an important role in neural

response.

3.3.1 Methods

The 3D hippocampus model (Section 2.1.2) was used for this study along with Poirazi's CA1 pyramidal cell (Section 2.3.1). The cell was shifted and positioned in the model such that the soma lay within the PC layer and between the middle two electrodes of the eight electrode stimulating array. However, the cell was slightly offset so that the electrodes were not overlapping the cell as shown in Fig. 3.5. In experimentation implanting the electrode over the cell would damage the neuron, while in simulation it would cause unrealistic voltages to be applied to the cell. Next, four different models were set up with an electrode implanted at a different depth in each (end of the stimulating electrode array in the: OR, PC, and two different depths in the LM). Those different depths are shown in Fig. 3.5. The multi-scale modeling methodology described in section 2.4 was used to determine the necessary amplitude of input current to cause an action potential within the cell (the threshold stimulation level). A biphasic current pulse across the two adjacent middle electrodes with a pulse duration of 1 ms was used.

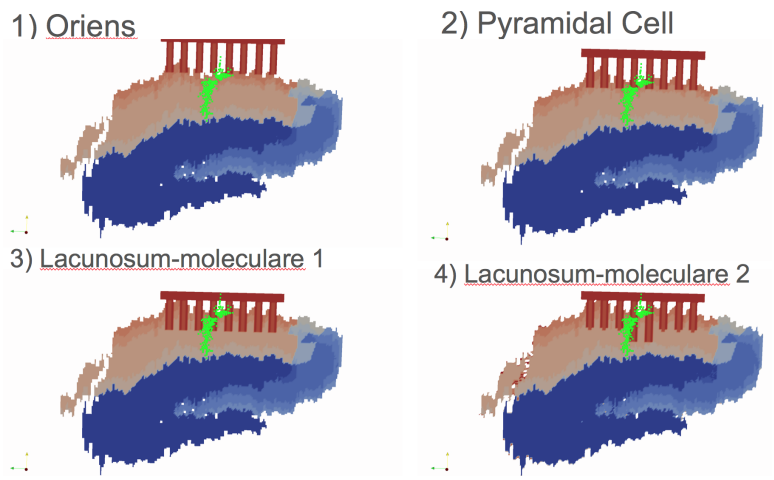

Figure 3.4: Slice through the model showing electrode depths. There were four different experiments run, with the tip of the electrode positioned in 1) the Oriens layer, 2) the Pyramidal Cell layer, and 3) and 4) at two depths within the Lacunosum-moleculare layer.

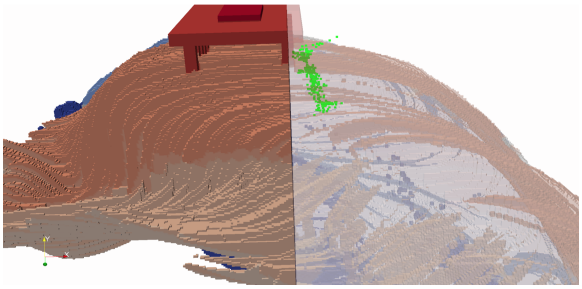

Figure 3.5: Electrode and neuron positioning within the model

3.3.2 Results

An admittance method simulation was run for each of the depths. Fig. 3.6 shows the admittance method potential field results with the electrode implanted at the PC layer and a stimulation amplitude of 100 μA. The dots represent the locations of the center of each compartment of the neuron. At each dot, the voltage was interpolated and applied to the cell. Similar results were obtained for the simulations at different depths.

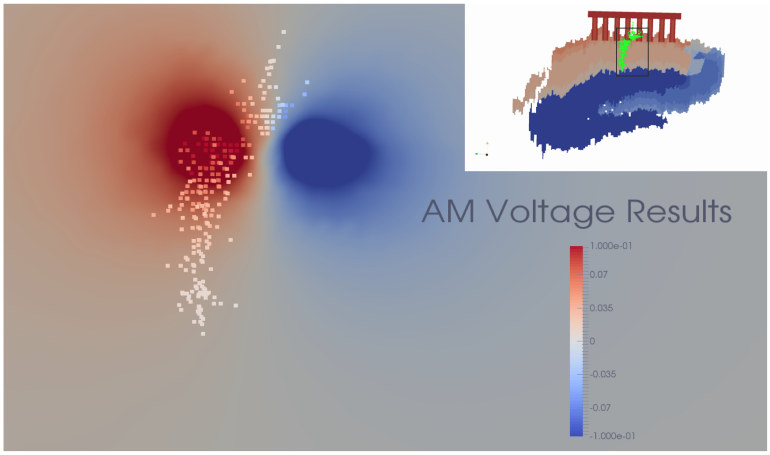

Figure 3.6: Admittance method potential field results with the electrode implanted at the PC layer. The dots represent the locations of the center of each compartment of the neuron. the subplot shows where the cutout of the potential field was taken with respect to the model.

Next, these voltages were applied to the neuron and the magnitude was varied to determine the threshold response level. Fig. 3.7a shows how as the depth of the electrode placement was varied, there was a clear increase in the necessary stimulation magnitude. Indeed there was an order of magnitude difference in the necessary input current between the

electrode placed in the OR ($\approx 8\ \mu A$) and the electrode placed in the lower LM ($\approx 80\ \mu A$). Likely causes of this difference include some combination of:

- The larger variation in resistivities through some regions of the hippocampus increasing the electric field within that region.
- The higher resistivity increasing the magnitude of the applied voltage.
- The difference in cell morphology as the dendrites are much more densely packed near the OR, and PC layers.
- Discrepancies in the conductances and governing equations of the dendrites and soma in the OR and PC layer vs. the apical dendrites in the LM layer.

Interestingly, there was also a significant latency in the cell response when the voltage at the soma for a threshold level stimulus input was plotted with respect to time for each experiment as shown in Fig. 3.7b. The greater the depth of electrode placement the longer the delay until the observed response of the soma. This result is intuitive because the electrode is causing a response at one of the lower compartments and it takes time for the signal to propagate through the cell to the soma. However, it is an important factor because neural prostheses are attempting to recreate specific spatial-temporal firing patterns and this indicates that both the spatial and temporal extent of the simulation will vary based on electrode placement.[1] These experiments indicate that the location of electrode placement can have a significant effect on spatial-temporal firing patterns and thus should be taken into consideration during any neural prostheses experiments within the hippocampus.

3.4 Ephaptic Coupling

Neural communication is complex, but essentially takes the form of spikes passed from one cell to another. Neural spikes are transmitted along an axon through the intake and release of charged potassium and sodium ions across the cell membrane. Additionally, each neuron contains a dendritic tree which connects to the dendrites of the surrounding

[1] Videos of the cell response are also available online at `http://tinyurl.com/adgilbert2016-supplementary`. There are videos which show the response for each experiment at its threshold stimulation level and at an amplitude of 50 μA of input current (where only the OR and PC cells are firing).

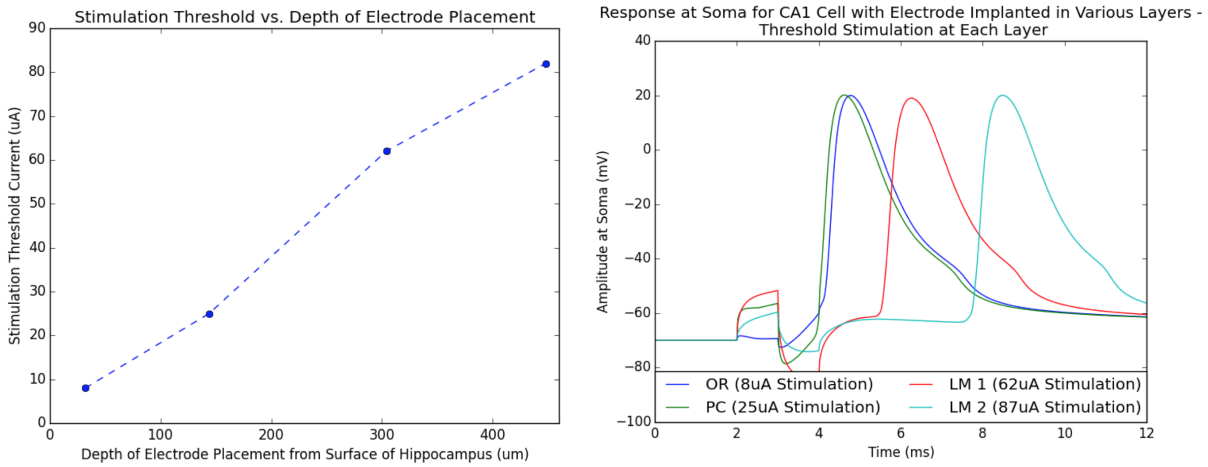

(a) The threshold stimulation level (in μA) for each electrode position.

(b) The response of each cell at its threshold stimulation level showing how latency of the cell response increases with increasing depth.

Figure 3.7: Difference in threshold and latency of response

neuron through synapses, where a synapse is the junction of two dendrites. When an action potential reaches the dendrites it causes the release of neurotransmitters into the synaptic cleft. These transmitters from the pre-synaptic neuron excite (or inhibit) the post-synaptic neuron through a small release of charged ions. This small release promotes (or hinders) a response in the post-synaptic neuron. This is known as synaptic coupling and is the most important mechanism of neural communication. In the hippocampus each pyramidal cell has approximately 30,000 synapses meaning there is a diverse and large set of inputs to each neuron at any given point in time [24].

However, a different mechanism, ephaptic coupling, has also been shown to play a role in neural communication [25] [26] [27]. As described above, an action potential works through the transmission of ions across the neuron membrane. These ions are released or extracted from the extracellular space which is shared with nearby neurons. In a densely packed environment, the influx of these charged ions can cause a change in the local field potential of the surrounding neurons, which may in turn change the activation threshold of those nearby neurons. Because a change in one neuron may induce a change in the others, those neurons are ephaptically coupled. This mechanism is separate from electric synapses which is when the membranes of two neurons are physically connected.

Ephaptic coupling was first described by Katz and Schmitt in 1940 [28]. They found

that ephaptic coupling by itself has too small of an effect to cause excitation of adjacent cells, at least in the majority of cases within the brain, a result confirmed by [29] [25] [26]. In some specific regions of the brain ephaptic coupling can cause a neuron to fire [27] or completely inhibit firing [33], but in these cases the fibers are often even more densely packed than in the hippocampus, and unmyelinated. In the majority of cases, including the hippocampus, it simply causes a change in the neural threshold of stimulation with the polarization of the "receiving cell" being inverse to the polarization experienced by the firing or "transmitting cell" (as the firing axon's membrane is depolarizing there is a hyperpolarizing effect on the local field potential). A difference of up to 20% has been observed in the response threshold of neurons due to ephaptic coupling [28]. The effect appears to have the greatest magnitude within the perisomatic region (30 — 40 μm from the soma) [29].

Other studies looking at how local electric fields from neural spiking effected firing patterns found that even small electric fields could generate a phase difference in temporal spiking patterns across the hippocampus. The generated phase difference increased by a factor of 10 from the PC layer to the LM [26]. These studies showed that the resting potentials of pyramidal neurons are ephaptically coupled together, inducing a synchronization in firing rate across the population [25] [26] [30] [31]. Meanwhile, a separate study found that memory formation in humans is tightly correlated with this synchronization [32] showing that ephaptic interactions could be especially important for a memory enhancement prosthetic as is the goal of the simulations presented here.

Ephaptic coupling clearly plays a role in determining the spatial-temporal spiking pattern of pyramidal cells in the hippocampus. However, it is unclear how that effect would change the response of neurons to suprathreshold extracellular (rather than synaptic) stimulation — Anastassiou *et al.* [26] showed synchronization with current clamps applied to 4 adjacent cells but this effect is different from an applied potential field. Therefore several stimulation cases were set up using the models described above to test the effects of ephaptic coupling.

3.4.1 Methods

The traditional mechanism for multi-scale modeling is described in Section 2.4 and Fig. 2.6. For the study on ephaptic coupling this methodology was modified. The modifications

are shown in Fig. 3.8. First, rather than just one cell placed in the model, a series of cells were positioned next to each other. One was the ”transmitting cell” and the others were ”receiving cells.” As in the original setup, a biphasic current pulse was input at the location of the electrodes. An admittance method simulation was run and the voltage field was extracted and applied to the transmitting neuron.However, then the membrane current was extracted from each compartment of the neuron cell at each timestep and that membrane current was used to set up a new admittance method simulation with the membrane current as a series of current sources at the locations in the mesh closest to the center of each compartment. The voltage field was extracted from that simulation as well. Finally a) the voltage field from the original simulation and b) the combined field from the original simulation and the new ephaptic simulation were applied to the receiving neurons. The difference in the receiving neuron response between a) and b) revealed the effects of ephaptic coupling.

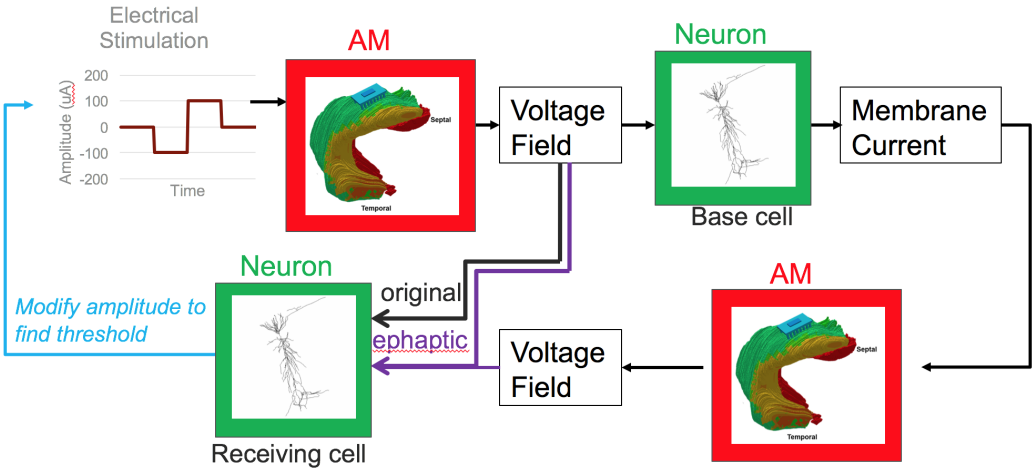

Figure 3.8: Ephaptic coupling simulation methodology showing how this methodology split from the original multiscale methodology by extracting current from the neuron model and using those a current sources in a new admittance method model then combining the two fields.

For this study the 3D hippocampus model and the CA1 Pyramidal cell models were used. A 100μA biphasic current pulse was input across the four pairs of adjacent stimulating electrodes as input to the model. The magnitude of the current was subsequently adjusted for a threshold response in the corresponding cells. The cells were placed as

shown in Fig. 3.9 where the background slice through the hippocampus shows placement with respect to the electrode. Each point represents the center of a neuron compartment, while the different colors represent five different cells. The transmitting cell is shown in black with the other colors representing receiving cells. Table 3.2 shows the distance between each of the receiving cells and the transmitting cell.

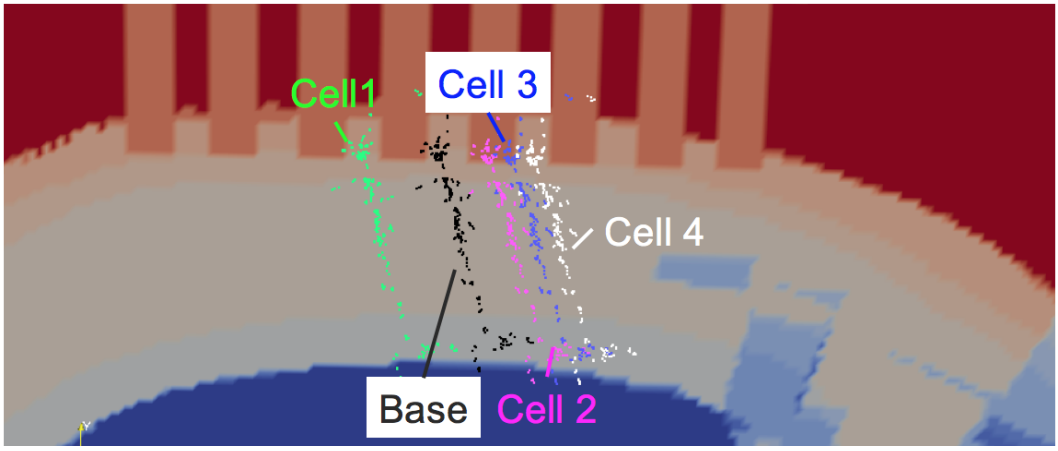

Figure 3.9: Cell placement for studying ephaptic coupling. Each color represents a different cell

Cell	Distance (μm)
1	186
2	147
3	186
4	229

Table 3.2: Distance between transmitting cell and receiving cells

3.4.2 Results

Preliminary results from the first few steps of the ephaptic simulation methodolgy are shown in Figs. 3.10, 3.11, and 3.12. Fig. 3.10 shows the voltage field generated from the original stimulus pulse. The field shows the biphasic nature of the stimulation current (positive and negative current on adjacent electrodes). This field was first applied to the transmitting cell (black).

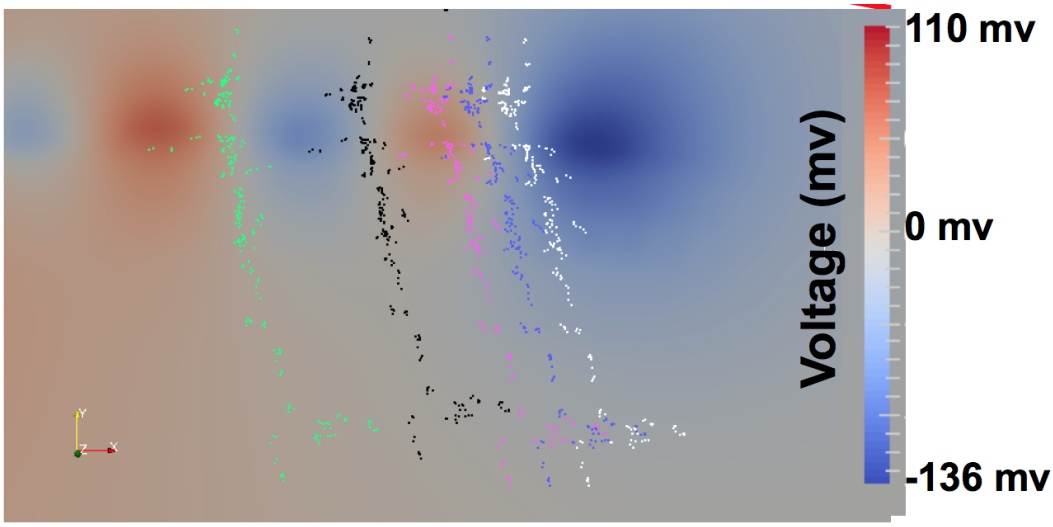

Figure 3.10: Voltage field from the original electrical stimulation

The transmitting cell fired from the applied stimulation and the membrane current through each compartment in the cell during the firing event was extracted. The current from five different compartments through the cell is shown in Fig. 3.11. The original synchronized pulses in the current occuring at approximately 2 and 3 ms are the response of the cell due to the applied stimulus voltage. The remaining series of spikes represent the action potential traveling through the cell The shape of the current shows the successive depolarization and repolarization of the cell membrane and how the action potential originates near the soma and travels down through the dendritic tree (the spike does not reach Apical Dendrite[101] in the 12 ms shown on the plot). When this current was extracted and set up as current sources in a new admittance method simulation, the resulting voltage field at one timestep is shown in 3.12. In this field several of the cell compartments are firing and the plot shows the resulting effect on the voltage field that this firing would cause.

Due to the variation in the field from ephaptic effects, a change in threshold was observed for each of the receiving cells. Those changes are shown in Table 3.3, where the change in threshold represents the change in the input current through the electrodes necessary to obtain a response in each cell. The difference in magnitude does not exactly correspond to the percentage difference because each cell had a different original firing threshold that depended on its location with respect to the electrode. All cells were positioned farther away along the z-axis compared to the position shown in Fig. 3.5 which is

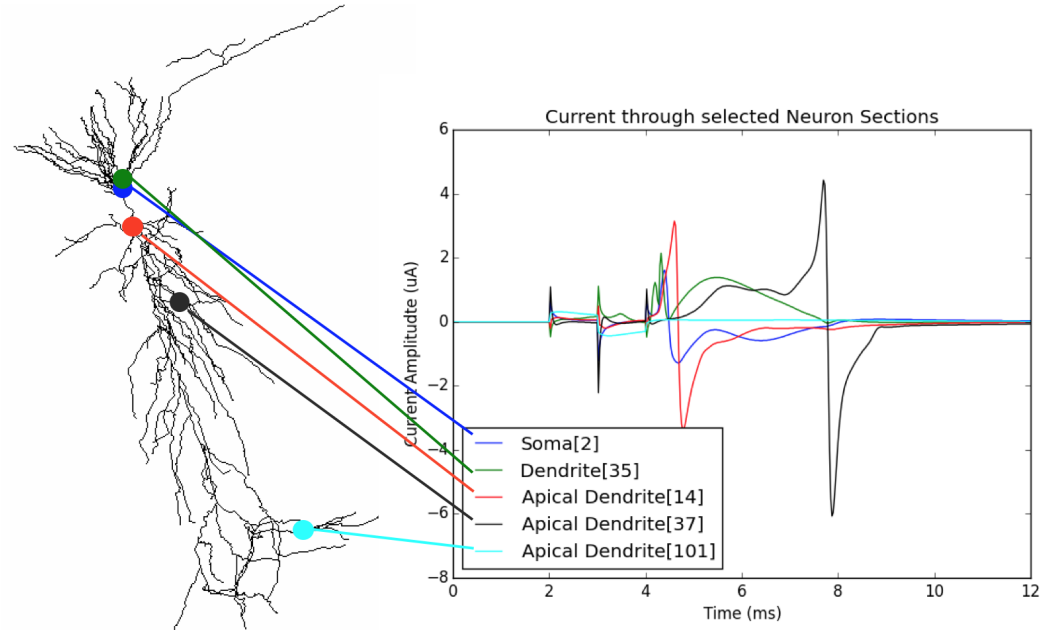

Figure 3.11: Membrane current extracted from several compartments of the transmitting cell

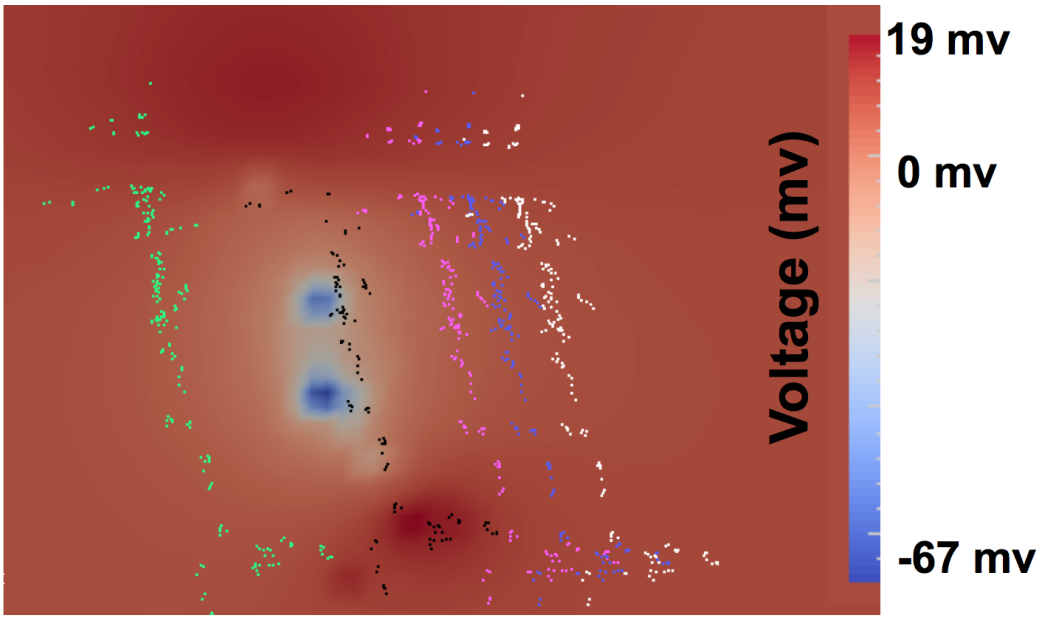

Figure 3.12: Voltage field from the firing of the transmitting cell

the reason for the much higher input current than in previous studies.

This table shows that there was about a 5% change in the necessary current regardless of the cell position. However, this effect could be either inhibitory or excitatory depending on the cell position with respect to the electrode. Although this effect is small, this model

Cell	Change in Threshold	
	Magnitude (uA)	Percent
1	-22	-4.9%
2	+17	+5.6%
3	+20	+4.9%
4	-22	-5.1%

Table 3.3: Change in necessary input current to induce a response in each cell when including the ephaptic effects

includes the change in threshold that would be incurred from including the current output from just one cell. The next step is to perform a similar study to analyze how an entire network of cells could change firing patterns.

3.5 A Bi-directional Communication System

While the method described above is an effective method for a preliminary study of ephaptic coupling and gives a good idea that there is an effect which should be included in computational models of neural stimulation, there are several flaws in the approach. The main flaw is that the method simulates for the entire duration of the simulation with no communication among the methods between two time-steps.In other words, it does not include updates of the membrane current based on ephaptic changes in the voltage fields and vice versa. Although this gives some idea of how the fields would change with the effects of ephaptic coupling it is a work-around rather than a system level approach.

A second problem is that membrane currents are applied only to the nearest node. Meanwhile voltages are interpolated at the exact location of the neuron compartment. While the nearest node is accurate enough to provide a rough estimation of ephaptic effects, it should also be interpolated such that it is applied at the exact location.

To remedy this, and include updates of ephaptic effects in every time-step, a bidirectional communication system between neuron and the admittance method was constructed. The system implemented was similar to the communication described above, just every timestep. In other words, the Neuron simulation extracts the membrane current from each compartment of each cell and passes the information to the Admittance Method. Meanwhile, the admittance method extracts the voltage at the center of each neuron compartment and passes the information to Neuron. This setup is shown in 3.13.

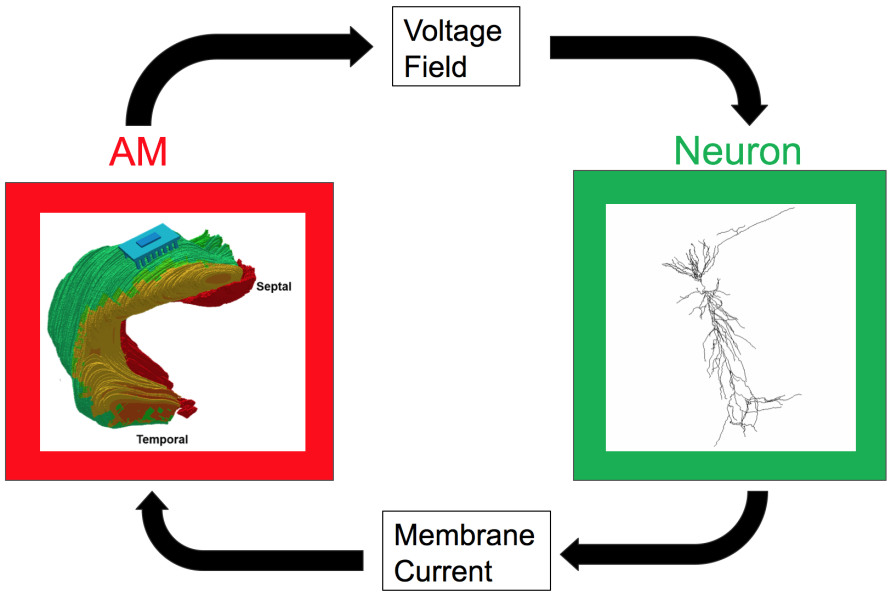

Figure 3.13: Bidirectional communication: Neuron passes the extracted membrane currents while the admittance method passes the extracted voltages

This effort was conducted in partnership with Dr. Ted Berger's group at the University of Southern California. The intermediary files to conduct the extraction of membrane current from a network of neurons and the application of the extracellular potential was implemented by Phillip Hendrickson and is described in [34].

The software to extract the relevant voltage fields and apply the extracted current was written in cooperation with Kyle Loizos. The modifications consisted of several steps, described below:

- Meshing:
  - The model is initialized such that the entire area where a neural network may be located is not meshed. While this slows down the simulation it presents a solution to the problem of just applying a current source to the nearest node. Instead, the current from each compartment is divided based on its distance to the 8 nodes of the voxel it is inside of, and a proportional current is applied to each of these nodes.The overall current emitted from the voxel should appear equivalent to a source placed at the interpolated location. This means that each of those 8 nodes must be present within the model and thus no meshing can occur in those locations.

- Admittance Method initialization:
  - Read in neuron locations. Initialize a class used to store the locations of each Neuron segment as well as arrays to contain the present current and voltages at that segment. The program always reads and writes sequentially assuming all values are in the same order as the initial location file.
- Admittance Method loop:
  - During each timestep the method reads in the new current file from Neuron. These currents are distributed as described above and added to the I vector (in the G $\times$ V = I system described in Section 2.2.2) at the correct matrix locations.
  - The system solves as usual
  - The system interpolates the voltage at the center of each neuron compartment and exports it to the Neuron simulation. Again this is made significantly easier since the system is assured of having the 8 surrounding nodes to each neuron compartment based on the meshing restrictions in place.
  - The system pauses the loop until it is able to read in the next current file.

This sequence was successfully implemented so that bidirectional communication between the two solvers is now possible. Initial results and demonstrations are currently in progress.

CHAPTER 4

CONCLUSION

The models and simulations in this work presented a strategy for modeling the electrical interaction between a neural prosthetic and the rat hippocampus. First, several models were implemented from other published studies. These models included several tissue models used to describe the propagation of current through the hippocampus and a neuron model to simulate neural actication due to this applied current. The admittance method was used to simulate for the current propagation, while Neuron software was used to simulate the complex behavior of neurons. Using this software a multi-scale modeling framework was developed which allowed the combination of these two elements to simulate neural response in a particular location of the hippocampus due to applied stimulation. Experiments were run to determine the effects of model capacitance, resistivity variations, changes in the depth of electrode placement, and ephaptic coupling. Results showed that capacitance was negligible, varying resistivity did have an effect on the movement of current through the model, the threshold of neural activation increased with increasing electrode depth, and including ephaptic coupling within the model would change those thresholds. Finally, a framework for a bi-directional communication system between the admittance method and neuron was implemented.

Additional steps can be taken to extend the model in this study. For example, while large-scale complex neural networks have been implemented for similar studies they were not implemented for those shown here. Implementing a network could provide valuable new information regarding the effects of electrical stimulation on entire sections of the hippocampus rather than just local regions.

Creating the set of multi-scale models of the hippocampus is just one of the methods that could be implemented to improve understanding of hippocampus function and future

direction of neural prostheses. However, through this study, I have presented a set of predictive tools to help with progressing a prosthesis to full functionality and safety. Having a set of simulation models with the complexity necessary for accurately predicting the behavior resulting from an applied stimulus can help with efficiently modifying existing designs and optimizing stimuli prior to experimentation.

APPENDIX A

ANALYSIS OF THE QUASI-STATIC APPROXIMATION

A brief analysis of Maxwell's equations describing the propagation of electromagnetic fields shows that capacitance should have a very limited effect. Starting by describing the curl of the magnetic field:

$$\bigtriangledown \times \vec{H} = \vec{J_c} + \frac{\partial \vec{D}}{\partial t} \tag{A.1}$$

Using $\vec{J} = \sigma \vec{E}$ and converting to the frequency domain gives:

$$\bigtriangledown \times \vec{H} = \sigma \vec{E} + j\omega \vec{D} \tag{A.2}$$

Finally, using $\vec{D} = \epsilon_r \epsilon_0 \vec{E}$ and combining yields:

$$\bigtriangledown \times \vec{H} = (\sigma + j\omega \epsilon_R \epsilon_0)\vec{E} \tag{A.3}$$

$\sigma = .3S/m$ is a typical published conductivity value often used for neural simulations. While there is some variation in conductivity with frequency, it is usually negligible. Meanwhile, ϵ_r is usually based off the literature study on permittivity values performed by Gabriel et al. in 1996 [22] (see Fig. A.1) and would be $\approx 1.5e5$ at 1 kHz. Based on these values, conductivity would be about 400 times larger than permittivity, indicating that permittivity is negligible in the determination of the magnitude of electromagnetic fields for low frequencies.

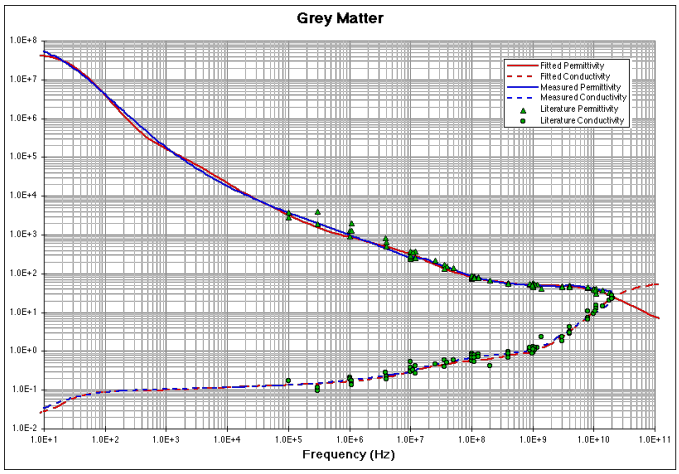

Figure A.1: Permittivity of Grey Matter at various frequencies. Image taken from `http://niremf.ifac.cnr.it/docs/DIELECTRIC/AppendixC.html`. Data from Gabriel et al. 1996 [22]

REFERENCES

[1] D. S. Gray, "Review of subject Slow-to-recover severe traumatic brain injury : a review of outcomes and rehabilitation effectiveness," *Brain Inj.*, vol. 14, 2000.

[2] P. J. Hendrickson, G. J. Yu, D. Song, and T. W. Berger, "A Million-Plus Neuron Model of the Hippocampal Dentate Gyrus: Critical Role for Topography in Determining Spatiotemporal Network Dynamics," *IEEE Trans. Biomed. Eng.*, vol. xx, no. xx, p. in press, 2015.

[3] T. W. Berger, D. Song, R. H. M. Chan, V. Z. Marmarelis, J. Lacoss, J. Wills, R. E. Hampson, S. a. Deadwyler, and J. J. Granacki, "A hippocampal cognitive prosthesis: Multi-input, multi-output nonlinear modeling and VLSI implementation," *IEEE Trans. Neural Syst. Rehabil. Eng.*, vol. 20, no. 2, pp. 198–211, 2012.

[4] H. Xu, M.-c. Hsiao, D. Song, and T. W. Berger, "Recording Place Cells from Multiple Sub-Regions of the Rat Hippocampus with a Customized Micro-Electrode Array," *36th Annu. Int. Conf. IEEE Eng. Med. Biol. Soc.*, pp. 4876–4879, 2014.

[5] T. W. Berger, R. E. Hampson, D. Song, A. Goonawardena, V. Z. Marmarelis, and S. A. Deadwyler, "A cortical neural prosthesis for restoring and enhancing memory," *J. Neural Eng.*, vol. 8, no. 4, p. 046017, 2011. [Online]. Available: http://stacks.iop.org/1741-2552/8/i=4/a=046017?key=crossref.968733ae620adc527b829d6f712ed0c7

[6] P. Poirazi, T. Brannon, and B. W. Mel, "Arithmetic of subthreshold synaptic summation in a model CA1 pyramidal cell," *Neuron*, vol. 37, no. 6, pp. 977–987, 2003.

[7] N. T. Carnevale and M. L. Hines, "The NEURON Book," *Neuron*, vol. 30, no. 2, p. 457, 2006. [Online]. Available: http://books.google.com/books?hl=en{&}lr={&}id=YzcOyjKBPHgC{&}oi=fnd{&}pg=PA1{&}dq=The+Neuron+Book{&}ots=Ki6EKu{_}ZLd{&}sig=3Cd1R026GoIeT59HkXyV-xHm7Yo

[8] C. J. Cela, "A Multiresolution Admittance Method for Large-Scale Bioelectromagnetic Interactions," Ph.D. dissertation, North Carolina State University, 2014.

[9] L. J. Kjonigsen, T. B. Leergaard, M. P. Witter, and J. G. Bjaalie, "Digital atlas of anatomical subdivisions and boundaries of the rat hippocampal region," *Front. Neuroinform.*, vol. 5, no. April, p. 2, 2011. [Online]. Available: http://www.frontiersin.org/neuroinformatics/10.3389/fninf.2011.00002/full

[10] D. Ropireddy, S. E. Bachus, and G. A. Ascoli, "Non-homogeneous stereological properties of the rat hippocampus from high-resolution 3D serial reconstruction of thin histological sections," *Neuroscience*, vol. 205, pp. 91–111, 2012. [Online]. Available: http://dx.doi.org/10.1016/j.neuroscience.2011.12.055

[11] L. López-Aguado, J. M. Ibarz, and O. Herreras, "Activity-dependent changes of tissue resistivity in the CA1 region in vivo are layer-specific: Modulation of evoked potentials," *Neuroscience*, vol. 108, no. 2, pp. 249–262, 2001.

[12] C. Bingham, K. Loizos, Y. Guo, G. J. Yu, P. J. Hendrickson, J.-m. C. Bouteiller, G. Lazzi, and T. W. Berger, "Multi-Scale Simulation of ElectrodeStimulation in the Dentate Gyrus," in *Poster Present. 44th Soc. Neurosci.*, Washington, D.C., 2014.

[13] D. W. Armitage, H. H. LeVeen, and R. Pethig, "Radiofrequency-induced hyperthermia: computer simulation of specific absorption rate distributions using realistic anatomical models," *Phys. Med. Biol.*, vol. 28, no. 1, pp. 31–42, 1983.

[14] C. J. Cela, R. C. Lee, and G. Lazzi, "Modeling cellular lysis in skeletal muscle due to electric shock." *IEEE Trans. Biomed. Eng.*, vol. 58, no. 5, pp. 1286–93, 2011. [Online]. Available: http://www.ncbi.nlm.nih.gov/pubmed/21216705

[15] F. Rattay, "Analysis of Models for External Stimulation of Axons," *IEEE Trans. Biomed. Eng.*, vol. 33, no. 10, pp. 974–977, 1986.

[16] A. L. Hodgkin and A. F. Huxley, "A quantitative description of membrane current and its application to conduction and excitation in nerve," *Bull. Math. Biol.*, vol. 52, no. 1-2, pp. 25–71, 1990.

[17] R. Plonsey and D. B. Heppner, "Considerations of quasi-stationarity in electrophysiological systems," *Bull. Math. Biophys.*, vol. 29, no. 4, pp. 657–664, 1967.

[18] C. Bédard, H. Kröger, and A. Destexhe, "Modeling extracellular field potentials and the frequency-filtering properties of extracellular space." *Biophys. J.*, vol. 86, no. 3, pp. 1829–42, 2004. [Online]. Available: http://www.sciencedirect.com/science/article/pii/S0006349504742502

[19] J. G. Stinstra and M. J. Peters, "The volume conductor may act as a temporal filter on the ECG and EEG," *Med. \& Biol. Eng. \& Comput.*, vol. 36, no. November, pp. 711–716, 1998.

[20] C. Butson and C. C. McIntyre, "Tissue and electrode capacitance reduce neural activation volumes during deep brain stimulation," *October*, vol. 141, no. 4, pp. 520–529, 2008.

[21] C. A. Bossetti, M. J. Birdno, and W. M. Grill, "Analysis of the quasi-static approximation for calculating potentials generated by neural stimulation," *J Neural Eng*, vol. 5, no. 1, pp. 44–53, 2008. [Online]. Available: http://www.ncbi.nlm.nih.gov/entrez/query.fcgi?cmd=Retrieve{&}db=PubMed{&}dopt=Citation{&}list{_}uids=18310810

[22] C. Gabriel, "Compilation of the Dielectric Properties of Body Tissues at RF and Microwave Frequencies," *Tech. Report, Dep. Physics, King's Coll. London*, vol. Report No., no. June, p. 21, 1996. [Online]. Available: www.dtic.mil/cgi-bin/GetTRDoc?AD=ADA303903

[23] D. A. Henze and G. Buzsáki, "Action potential threshold of hippocampal pyramidal cells in vivo is increased by recent spiking activity," *Neuroscience*, vol. 105, no. 1, pp. 121–130, 2001.

[24] M. Megías, Z. Emri, T. F. Freund, and a. I. Gulyás, "Total number and distribution of inhibitory and excitatory synapses on hippocampal CA1 pyramidal cells." *Neuroscience*, vol. 102, no. 3, pp. 527–540, 2001.

[25] C. A. Anastassiou, S. M. Montgomery, M. Barahona, G. Buzsaki, and C. Koch, "The Effect of Spatially Inhomogeneous Extracellular Electric Fields on Neurons," *J. Neurosci.*, vol. 30, no. 5, pp. 1925–1936, 2010. [Online]. Available: http://www.jneurosci.org/cgi/doi/10.1523/JNEUROSCI.3635-09.2010

[26] C. a. Anastassiou, R. Perin, H. Markram, and C. Koch, "Ephaptic coupling of cortical neurons," *Nat. Neurosci.*, vol. 14, no. 2, pp. 217–223, 2011. [Online]. Available: http://dx.doi.org/10.1038/nn.2727

[27] H. Bokil, N. Laaris, K. Blinder, M. Ennis, and A. Keller, "Ephaptic interactions in the mammalian olfactory system," *J. Neurosci.*, vol. 21, no. 20, p. RC173, 2001. [Online]. Available: http://www.ncbi.nlm.nih.gov/pubmed/11588203

[28] B. Katz and O. H. Schmitt, "Electric interaction between two adjacent nerve fibres." *J. Physiol.*, vol. 97, no. 4, pp. 471–88, 1940. [Online]. Available: http://www.pubmedcentral.nih.gov/articlerender.fcgi?artid=1393925{&}tool=pmcentrez{&}rendertype=abstract

[29] G. R. Holt and C. Koch, "Electrical interactions via the extracellular potential near cell bodies," *J. Comput. Neurosci.*, vol. 6, no. 2, pp. 169–184, 1999.

[30] E. Park, E. Barreto, and B. Gluckman, "A model of the effects of applied electric fields on neuronal synchronization," *J. Comput. . . .*, vol. 19, no. 1, pp. 53–70, 2005. [Online]. Available: http://link.springer.com/article/10.1007/s10827-005-0214-5

[31] T. Radman, Y. Su, J. H. An, L. C. Parra, and M. Bikson, "Spike timing amplifies the effect of electric fields on neurons: implications for endogenous field effects." *J. Neurosci.*, vol. 27, no. 11, pp. 3030–3036, 2007.

[32] U. Rutishauser, I. B. Ross, A. N. Mamelak, and E. M. Schuman, "Human memory strength is predicted by theta-frequency phase-locking of single neurons," *Nature*, vol. 464, no. 7290, pp. 903–907, 2010. [Online]. Available: http://www.nature.com/doifinder/10.1038/nature08860

[33] H. Korn and H. Axelrad, "Electrical inhibition of Purkinje cells in the cerebellum of the rat." *Proc. Natl. Acad. Sci. U. S. A.*, vol. 77, no. 10, pp. 6244–6247, 1980.

[34] P. J. Hendrickson and D. Song, "A Bi - Directional Communication Paradigm Between Parallel NEURON and an External Non - NEURON Process," in *Submitt. to Eng. Med. Biol. Soc. (EMBC), 2016*, Orlando, 2016.